Supplementary Materials for

"A two-track model for the spatiotemporal coordination of bacterial septal cell wall synthesis revealed by single-molecule imaging of FtsW"

Xinxing Yang[1*], Ryan McQuillen[1], Zhixin Lyu[1], Polly Phillips-Mason[2], Ana De La Cruz[1], Joshua W. McCausland[1], Hai Liang[3,5], Kristen E. DeMeester[3], Cintia C. Santiago[3], Catherine L. Grimes[3,4], Piet de Boer[2*], Jie Xiao[1*]

[1]Department of Biophysics and Biophysical Chemistry, Johns Hopkins School of Medicine, Baltimore, Maryland, 21205, USA.
[2]Department of Molecular Biology & Microbiology, School of Medicine, Case Western Reserve University, Cleveland, Ohio 44106-4960, USA.
[3]Department of Chemistry and Biochemistry, University of Delaware, 134 Brown Lab, Newark, Delaware 19716, USA.
[4]Department of Biological Sciences, University of Delaware, Newark, Delaware 19716, USA.
[5]Current address: Dermatology Branch, National Institute of Arthritis and Musculoskeletal and Skin Diseases, NIH, Bethesda, MD 20892, USA

*Correspondence and requests for materials should be addressed to X.Y. (email: novayang@gmail.com), P.d.B. (email: pad5@case.edu) and J.X. (email: xiao@jhmi.edu)

This PDF file includes:
Supplementary Figures 1 to 6
Supplementary Table 1 to 9
Supplementary Discussion
Captions for Movies S1 to S9
References

Other Supplementary Materials for this manuscript includes the following:
Movies S1 to S9

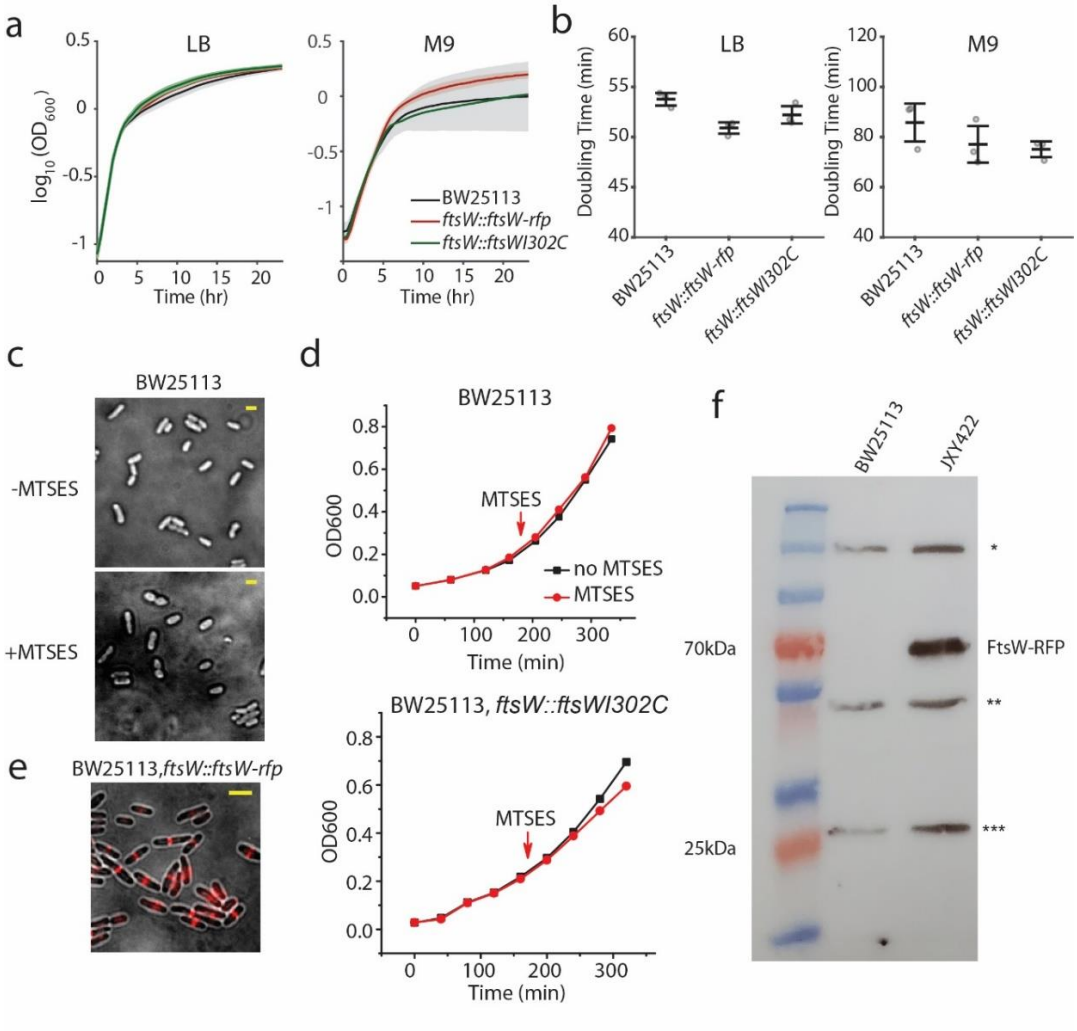

Supplementary Figure 1. **Characterizations of FtsW, FtsW^{I302C} and FtsW-TagRFP-t fusion proteins used in the study.**

a. Growth curves of BW25113 (*wt*), JXY422 (*ftsW-TagRFP-t*), and JXY559 (*ftsW^{I302C}*) cells in LB or M9-glucose medium. Data are presented as mean ± SEM. from three independent experiments. **b**. Doubling times of the three strains in LB and M9 calculated from growth curves in **a**. Data are presented as mean ± s.d. from three independent experiments. **c**. Snapshots of log phase BW25113 (*wt*) cells grown in M9 medium without (top panel) or with (bottom) MTSES. Scale bars:1 µm. **d**. Growth curves of BW25113 (*wt*) and JXY559 (*ftsW^{I302C}*) cells in M9 medium upon addition of MTSES in early log-phase. **e**. JXY422 (*ftsW-TagRFP-t*) cells showing the expected midcell localization of FtsW-TagRFP-t. Scale bar: 2µm. Micrographs in **c and e** are representative of three independent experiments. **g**. Immunoblot of FtsW-TagRFP-t using anti-TagRFP antibody. As expected, the FtsW-TagRFP-t band (~70kDa) is present in JXY422 but not in BW25113. Three non-specific bands (*, **, ***) are evident in both samples. Band*** migrates close to what would

be expected of free TagRFP-t. If the modestly increased intensity of band*** in the JXY422 sample were due to degradation of the full length FtsW-TagRFP-t, it would represent only a minor fraction (< 4%) of total FtsW-TagRFP-t. Cells were grown at room temperature (c, f, g), 30^{o}C (a, b), or 37^{o}C (e). MTSES was used at 0.1 mM in c and d; 1 mM in e.

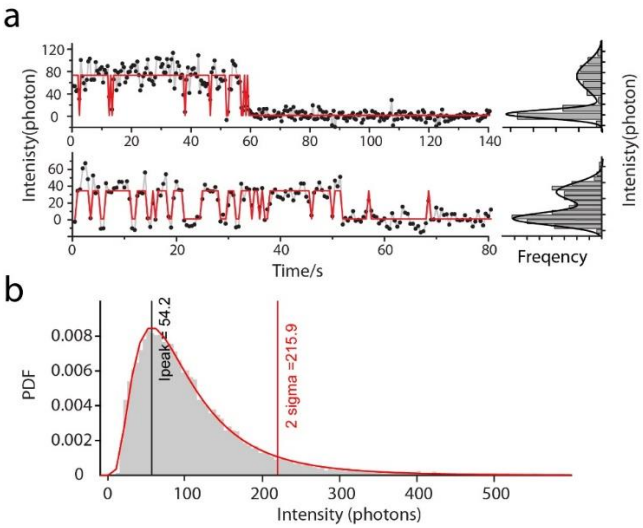

Supplementary Figure 2. **Example of single-particle intensity traces and allover intensity distribution of FtsW-RFP in BW25113 strain in M9-glucose medium.**

a. Intensity traces show single step photobleach and blinking behavior, which suggest they are single FtsW-RFP molecules. Intensity was subtracted by the average background and integrated over a 5-by-5 pixel region, and back-calculated to photon numbers using experimental camera setting (EmGain = 300, preAmp = 9.93, Quantum yield ~ 0.96). Intensity histograms are shown on the right. **b.** Probability density function (PDF) of all fluorescent spots in BW25113 strain expressing FtsW-RFP. Most of the spots are from single FtsW-RFP (~54 photons). To minimize the possibility of tracking multiple FtsW-RFP molecules at a time, we removed spots with intensity > 2 sigma (~4 molecules) prior to further analysis.

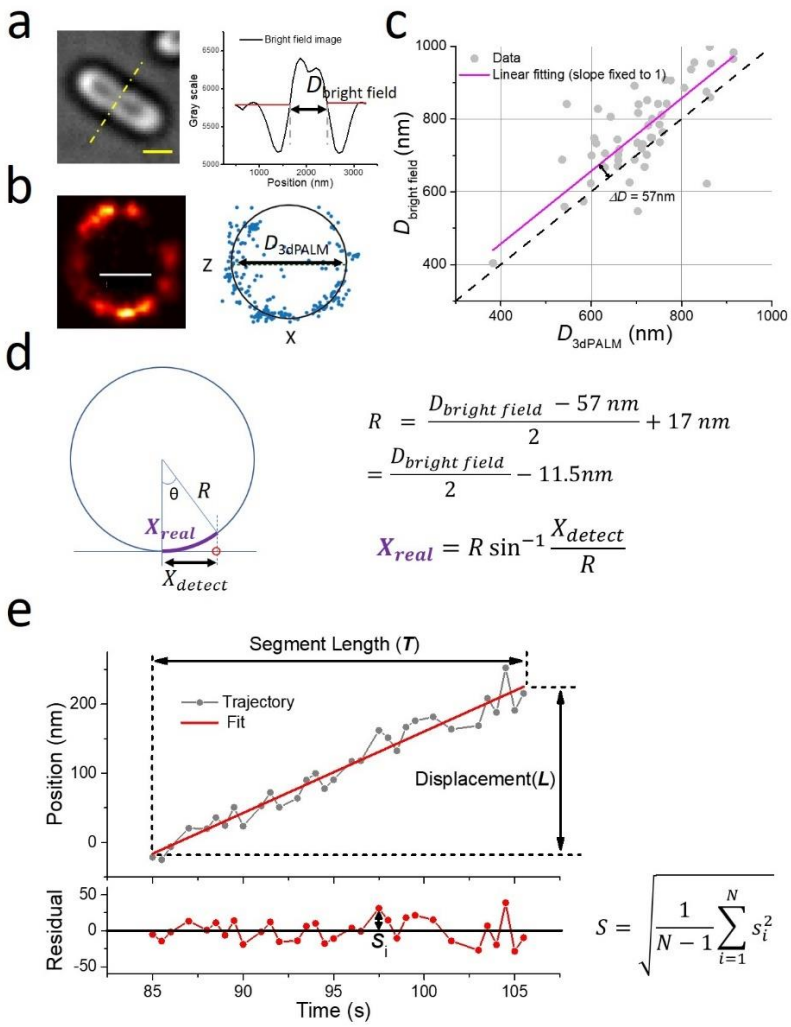

Supplementary Figure 3. **Custom-developed cell envelope unwrapping method to retrieve true coordinates of single molecules along the circumference of the curved cell surface**.

a. The apparent cell diameter ($D_{bright\ field}$, right panel) is measured using the intersections of the background signal (red line) with the cell profile (black curve) resulted from a line scan (yellow dashed line) of the cell's bright-field image (left panel). Scale bar: 1 μm. **b**. For each cell (BW25113/pJL005), the corresponding diameter of FtsZ ring (D_{3dPALM}) is measured using three-dimensional (3D) superresolution image of FtsZ-mEos3.2 (left) fit with a circle (right). Scale bar: 0.5 μm. **d**. The true cell radius (R, from cell center to the inner membrane) is calculated from $D_{bright\ field}$ subtracting the intersection and adding the distance between FtsZ ring and inner membrane (~ 17nm[1]). The 'true' coordinate X_{real} (purple arc) of a molecule along the circumference of the cell inner membrane is calculated using the true cell radius R and the detected X coordinate X_{detect} (bottom equation). **e**. One segment of a single FtsW-RFP trajectory along the circumference fits to

a line. The displacement (L) and the segment length (T) introduced in the Methods are labeled in the top panel. The noise level S is defined as the standard deviation of the residuals (s_i, bottom panel, Methods). **a and b.** Micrographs are representative of independent experiments. **c**. The apparent cell diameter $D_{bright\ field}$ is plotted against D_{3dPALM} from the same cell and fit with a line with a slope of 1 and intersection at 57nm (magenta line). **a, b, and c.** n = 52 cells with Z-ring.

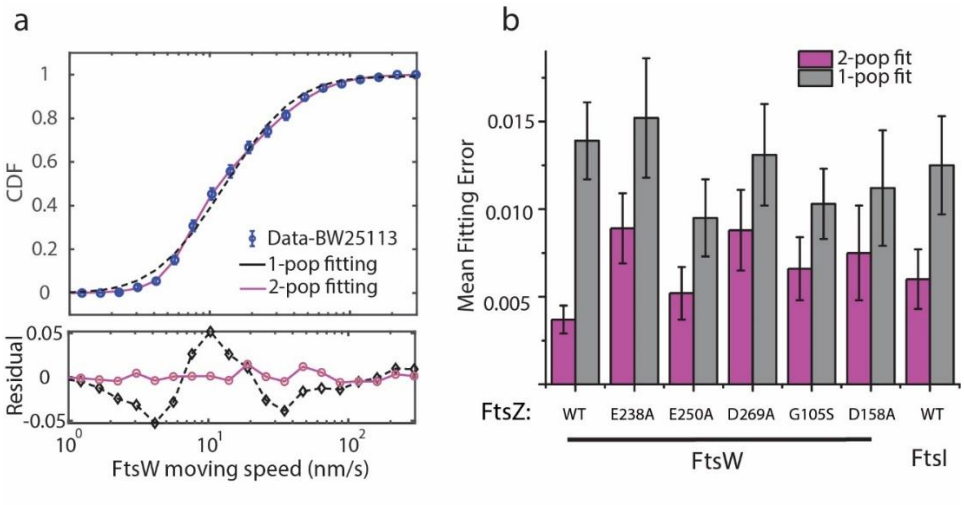

Supplementary Figure 4. **Single- or double-population fitting of the cumulative probability density of directional moving speed distribution**.

a. CDF curve of the directional moving speed of FtsW-RFP molecules in WT BW25113 cells (blue circles) was best fit by a double (solid magenta curve) instead of a single (dash gray curve) population (empirically using log-normal distribution to describe the long tail), as indicated by the residuals below. Error bars indicate SEM from bootstapping. **b.** Standard error of the mean of the fitting residuals from 1000 times bootstrapping (bottom panel in a) indicates that most CDF curves were best fit with two populations (magenta) in both BW25113 and FtsZ GTPase mutant cells. Data are presented as mean ± SEM. (For details regarding statistics and plot definitions see the “Statistics” subheading in “Methods”.)

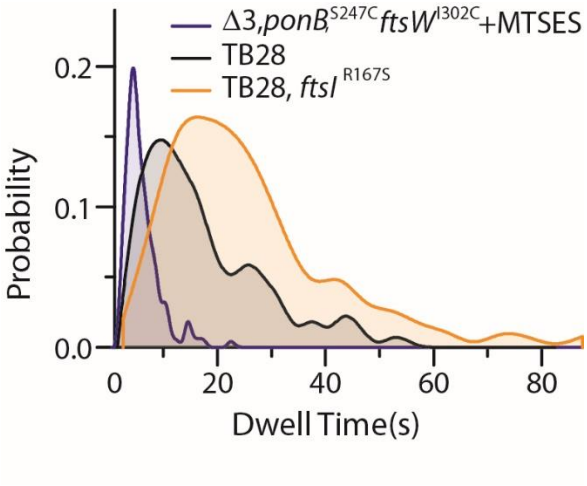

Supplementary Figure 5. Dwell time distribution of processive moving FtsW-RFP molecules at the division septum.

Black curve: Dwell time distribution of processive moving FtsW-RFP molecules in wildtype TB28 cells. Orange curve: Moving FtsW-RFP molecules display longer dwell times in cells of the FtsI SF mutant strain PM6 (TB28, *ftsI*^{R167S}). Blue curve: Inhibition of sPG synthesis (all PGTases) results in short dwell times. Note that the imaging conditions for each curve were identical, indicating that differences in these distributions were not due to different levels of photobleaching. The differences are rather more reflective of FtsW-RFP molecules spending more (orange) or less (blue) time than usual on the sPG-track (synthesizing sPG), rather than on the Z-track (tracking FtsZ filaments).

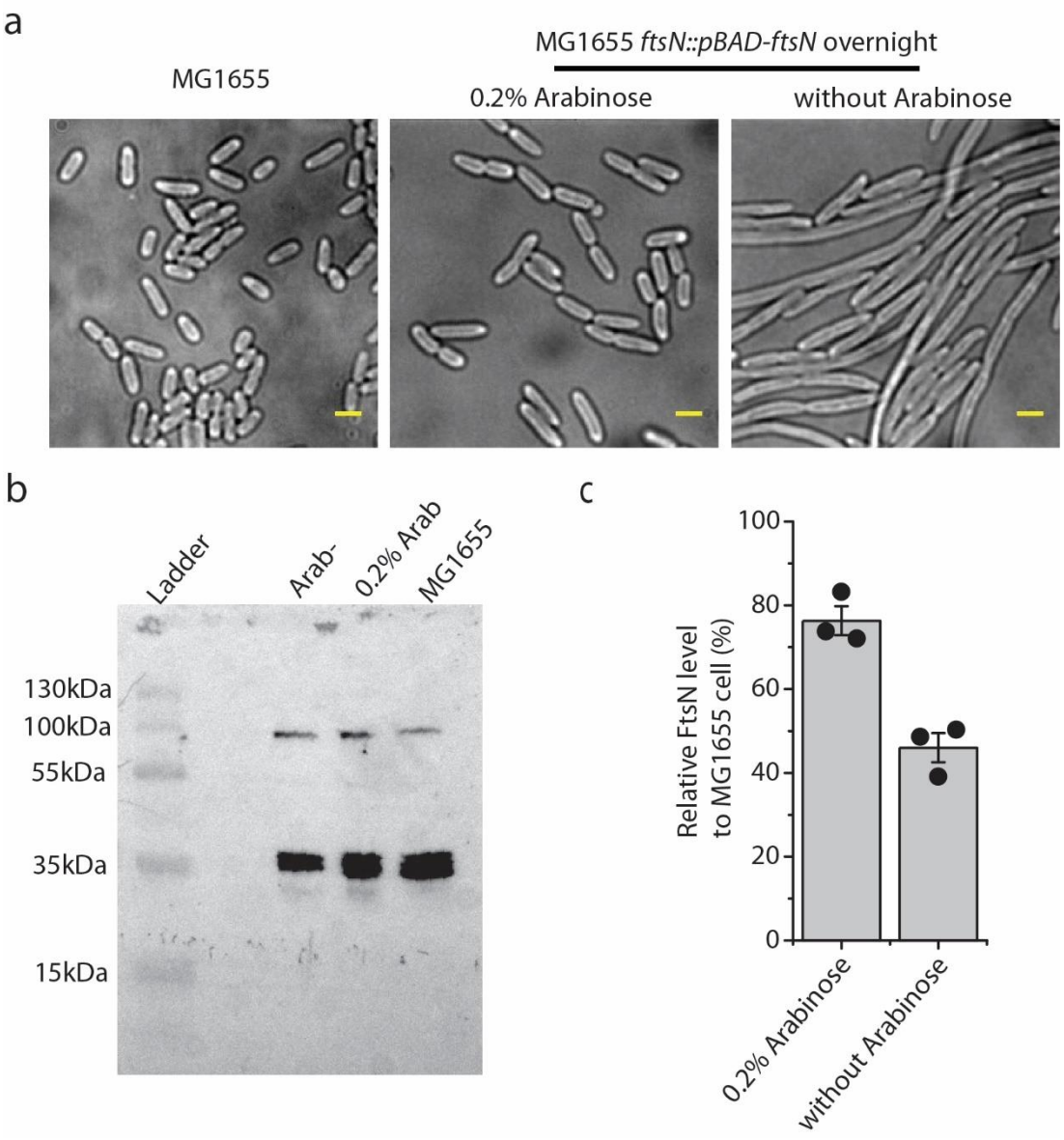

Supplementary Figure 6. Characterization of the FtsN depletion strain (EC1908).

a. Bright field cell images of *wt* strain MG1655 strain, and of the FtsN-depletion strain EC1908 grown in the presence ($FtsN^+$) or absence ($FtsN^-$) of 0.2% L-arabinose. Micrographs are are representative three independent experiments. Scale bar: 2µm. **b**. Representative immunoblot of FtsN (~35kDa) using anti-FtsN antiserum from Dr. David S. Weiss[2] from three independent sample sets. Slight degradation of FtsN during the experiment causes the multiple banding pattern. **c.** Quantification of the blots shows that the total FtsN level after overnight depletion decreases to ~ 45% of the WT cells. Cells were grown in M9-glucose medium overnight at room temperature to OD_{600} = 0.5-0.6. Data are presented as mean ± s.d. from three independent experiments.

Supplementary Table 1: Strains and plasmids used in the study

Strain	**Genotype**	**Reference/source**
BW25113	Δ*(araD-araB)567,* Δ*lacZ4787(::rrnB-3), rph-1,* Δ*(rhaD-rhaB)568, hsdR514*	3
BL17	TB28 *leu*::Tn10	4
BL167	TB28 *ftsB*^{E56A}	4
BL173	TB28 *ftsB*^{E56A} *ftsN*::*aph*	4
CH34*	TB28 *ftsN*::*aph*	5
EC1908*	MG1655 P_{BAD}::*ftsN*	2
HC532	MG1655 *lysA::frt ponA::frt pbpC::frt mtgA::frt ponB*^{S247C}	6
JXY001	BW25113 *ftsZ*^{G105S}(ts)	7
JXY002	BW25113 *ftsZ*^{E250A}	7
JXY003	BW25113 *ftsZ*^{D158A}	7
JXY005	BW25113 *ftsZ*^{E238A}	7
JXY006	BW25113 *ftsZ*^{D269A}	7
JXY263	BW27783 *ftsZ*::*ftsZ*55-56-*mNeonGreen*, P_{lac}::*ftsZ-tagRFP-t*	7
JXY304*	BW25113 *ftsW*::*aph*	This study
JXY422	BW25113 *ftsW-tagrfp-t*	This study
JXY559	BW25113 *ftsW*^{I302C}	This study
JXY564	MG1655 *lysA::frt ponA::frt pbpC::frt mtgA::frt ponB*^{S247C} *ftsW*^{I302C}	This study
JXY589	BW25113 *murJ*^{A29C}	This study
MG1655	*ilvG rfb*50 *rph*1	8
PM4	TB28 *ftsN*^{slm117} *ftsI*^{R167S}	This study
PM6	TB28 *ftsI*^{R167S}	This study
PM8*	TB28 *ftsI*^{R167S} *ftsN*::*aph*	This study
PM17	TB28 *ftsW*^{E289G}	This study
PM18	TB28 *ftsW*^{E289G} *ftsN*::*aph*	This study
TB28	MG1655 *lacIZYA*::*frt*	9
TB77	TB28 *ftsN*^{slm117} (*ftsN*::EZTnKan-2)	5
Plasmid	**Genotype**	**Reference/source**
pAD004	ColE1, *bla lacI*^{Q1} P_{T5lac}::*ftsW*^{I302C}*-tagRFP-t*	This study
pAD005	ColE1, *bla lacI*^{Q1} P_{T5lac}::*ftsW*^{I303C}*-tagRFP-t*	This study
pBAD33	pACYC, *cat araC* P_{BAD}::	10
pBBR1-KU	ColE1, *cat* P_{lac}::*amgK murU* (*P. putida* genes)	11

pBL145	pSC101, *aadA cI*^{ts} $P_{\lambda R}$::*ftsN*$^{1-90}$	4
pCH201	ColE1, *bla* ^{Q}*lacI*^{Q} P_{lac}::*gfp-ftsN*	12
pCH650	pACYC, *cat araC* P_{BAD}::*uppS*	This study
pDSW406	pACYC, *cat araC* P_{BAD}::*ftsW*	13
pGH33	ColE1, *aph* P_{BAD}::*spCas9*	A gift from Dr. Glenn Hauk
pGH34	pACYC, *cat* P_{BAD}::*sacB, sgRNA*	A gift from Dr. Glenn Hauk
pHC808	ColE1, *cat lacI*^{Q} P_{tac}::*uppS*	14
pJB007	ColE1, *cat lacI*^{Q} P_{T5lac}::*tagrfp-t-ftsI*	7
pJL005	ColE1, *bla lacI*^{Q} P_{T5lac}::*ftsZ-meos3.2*	15
pJL018	ColE1, *bla lacI*^{Q} P_{T5lac}:: *ftsW-tagRFP-t*	This study
pJM19	pACYC, *cat* P_{BAD}::*sacB, ftsW-sgRNA*	This study
pKD13	R6K, *bla frt::aph::frt*	3
pKD46	pSC101, *bla repA*^{ts}, *araC* P_{BAD}::*gam bet exo*	3
pXY018	ColEl, *cat lacI*^{Q} P_{T5lac}::*gfp-zapA*	7
pXY027	ColE1, *cat lacI*^{Q} P_{T5lac}::*ftsZ-gfp*	1
pXY253	ColE1, *cat lacI*^{Q} P_{T5lac}::*ftsW-tagRFP-t*	This study
pXY287	pACYC, *cat araC* P_{BAD}::*ftsW, sacB*	This study
pXY349	ColE1, *bla lacI*^{Q1} P_{T5lac}::*ftsW-tagRFP-t*	This study
pXY388	ColE1, *aph lacI*^{Q1} P_{T5lac}:: *tagRFP-t-ftsI*	This study
pXY437	ColE1, *bla lacI*^{Q1} P_{T5lac}::*ftsW*^{A301C}*-tagRFP-t*	This Study
pXY438	ColE1, *bla lacI*^{Q1} P_{T5lac}::*ftsW*^{L367C}*-tagRFP-t*	This study
pXY439	ColE1, *bla lacI*^{Q1} P_{T5lac}::*ftsW*^{E289G}*-tagRFP-t*	This study
pXY441	ColE1, *bla lacI*^{Q1} P_{T5lac}::*ftsW*^{S131C}*-tagRFP-t*	This study
pXY442	ColE1, *bla lacI*^{Q1} P_{T5lac}::*ftsW*^{S136C}*-tagRFP-t*	This study
pXY443	ColE1, *bla lacI*^{Q1} P_{T5lac}::*ftsW*^{L198C}*-tagRFP-t*	This study
pXY445	ColE1, *bla lacI*^{Q1} P_{T5lac}::*ftsW*^{L268A}*-tagRFP-t*	This study
pXY446	ColE1, *bla lacI*^{Q1} P_{T5lac}::*ftsW*^{L276C}*-tagRFP-t*	This study
pXY447	ColE1, *bla lacI*^{Q1} P_{T5lac}::*ftsW*^{L288C}*-tagRFP-t*	This study
pXY448	ColE1, *bla lacI*^{Q1} P_{T5lac}::*ftsW*^{A294C}*-tagRFP-t*	This study
pXY449	ColE1, *bla lacI*^{Q1} P_{T5lac}::*ftsW*^{L307C}*-tagRFP-t*	This study
pXY550	pACYC, *cat* P_{BAD}::*sacB, ftsWI302-sgRNA*	This study
pXY588	pACYC, *cat* P_{BAD}::*sacB, murJA29C-sgRNA*	This study
pXY677	ColE1, *cat lacI*^{Q} P_{T5lac}::*mNeonGreen-zapA*	This study

* Cells require a complementing plasmid or specific growth conditions for survival.

Supplementary Table 2: Primers used in the study

Primer	Sequence	Purpose
1	GAGGAGAAATTAACTACTAGTATGGTGTCTAAGGGCGAAGAGC	Amplification of *ftsW* gene for pXY349
2	CGGTGCCGGTGCCGGGCTACCACCGCCACCCTTGTACAGCTCGTCCATGCCA	
3	CCGGCACCGGCACCGGGCGGTGGCGGTAGCCGTTTATCTCTCCCTCGCC	Amplification of *tagrfp-t* gene for pXY349
4	GGTCGACCCTTAGCGGCCGCTTATCGTGAACCTCGTACAAACG	
5	ACTAGTAGTTAATTTCTCCTCTTTAATG	Amplification of the vector backbone for pXY349
6	GCGGCCGCTAAGGGTCG	
7	TGCCATACCGCGAAAGGTTTGTCAACATTCGATGGTGTCGGAATT	Mutagenesis of *lacI*^{Q} promotor for pXY349
8	AATTCCGACACCATCGAATGTTGACAAACCTTTCGCGGTATGGCA	
9	TTTTTTTAAGGCAGTTATTGGTGC	Amplification of the vector to swap *cat* to *bla*
10	ACGTCTCATTTTCGCCAAAAGTT	
11	GCGAAAATGAGACGTTTACCAATGCTTAATCAGTGAGG	Amplification of *bla* gene
12	ACTGCCTTAAAAAAACGCGGAACCCCTATTTGTTTA	
13	ACCCCAGTTCTTCGCCGATACAGGCGAAAATAAAGTCAGTG	Mutagenesis of *ftsW* for pAD004
14	CACTGACTTTATTTTCGCCTGTATCGGCGAAGAACTGGGGT	
15	CCAGTTCTTCGCCGCAAATGGCGAAAATAAAGTCAGTGTG	Mutagenesis of *ftsW* for pAD005
16	CACACTGACTTTATTTTCGCCATTTGCGGCGAAGAACTGG	
17	AGTTCTTCGCCGATAATGCAGAAAATAAAGTCAGTGTGCGC	Mutagenesis of *ftsW* for pXY437
18	GCGCACACTGACTTTATTTTCTGCATTATCGGCGAAGAACT	
19	CTTTGGTCGGGCACATCCCCGCCGCCGCG	Mutagenesis of *ftsW* for pXY438
20	CGCGGCGGCGGGGATGTGCCCGACCAAAG	
21	CGCTTCCGGCAGATACCCCAGTTTTTGTACCGA	Mutagenesis of *ftsW* for pXY439
22	TCGGTACAAAAACTGGGGTATCTGCCGGAAGCG	
23	GCGATGCCCCTTTAACGCAGCTACCCACTACCAG	Mutagenesis of *ftsW* for pXY441
24	CTGGTAGTGGGTAGCTGCGTTAAAGGGGCATCGC	
25	GAGATCGATCCAACGGCATGCCCCTTTAACCGAGC	Mutagenesis of *ftsW* for pXY442
26	GCTCGGTTAAAGGGGCATGCCGTTGGATCGATCTC	
27	ACCACCACCGTACCACAGTCTGGCTGTGCCAG	Mutagenesis of *ftsW* for pXY443
28	CTGGCACAGCCAGACTGTGGTACGGTGGTGGT	
29	CGCCGCGACCAAACGCCATGCACGATTGCGTTAACTGATAG	Mutagenesis of *ftsW* for pXY445
30	CTATCAGTTAACGCAATCGTGCATGGCGTTTGGTCGCGGCG	
31	CTTGCCCCCAACATTCGCCGCGACCAAACGCCA	

32	TGGCGTTTGGTCGCGGCGAATGTTGGGGGCAAG	Mutagenesis of *ftsW* for pXY446
33	GCGCTTCCGGCAGATACTCGCATTTTTGTACCGAGTTACCTAAAC	Mutagenesis of *ftsW* for pXY447
34	GTTTAGGTAACTCGGTACAAAAATGCGAGTATCTGCCGGAAGCGC	
35	AAAACTGGAGTATCTGCCGGAATGCCACACTGACTTTATTTTCGCC	Mutagenesis of *ftsW* for pXY448
36	GGCGAAAATAAAGTCAGTGTGGCATTCCGGCAGATACTCCAGTTTT	
37	CCACACCGACATACCCGCATTCTTCGCCGATAATGGCGAAAATAA	Mutagenesis of *ftsW* for pXY449
38	TTATTTTCGCCATTATCGGCGAAGAATGCGGGTATGTCGGTGTGG	
39	TTGGCTGTTTTGGCGTTTGTTTAACTTTAAGAAGGAGAATGAAC	Amplification of *sacB* gene for pXY287
40	CCGCTTCTGCGTTCTTTATTTGTTAACTGTTAATTGTCCTTGTT	
41	CGCCAAAACAGCCAAGCTTG	Amplification of the vector backbone for pXY287
42	AGAACGCAGAAGCGGTCTGA	
43	TTGAACAACGAGGCAATGAGTTTGCCCGTCTGGCGAAGGAGTTAGGTTGAGGAGCTGCTTCGAAGTTCCT	Knockout of *ftsW*
44	CAATCCACCGGTTCCGCCTGCCATCACCATTAATCGCTTTCCTTGACCACTAGCTGCTTCGAAGTTCCT	
45	GTGCACATTATACGAGCCGATGA	Amplification of the vector backbone for pJM19
46	ATCATGGCGACCACACCCGTCCTGTGGATCCTCTAC	
47	TCGTATAATGTGCACAGGTTCACGATGAGTGGTCAGTTTTAGAGCTAGAAATAGCAAGTTAA	Amplification of the sgRNA for pJM19
48	CGGCGTAGAGGATCCACAGGACGGGTGTGGTCGC	
49	TCGTATAATGTGCACCCATTATCGGCGAAGAACTGGTTTTAGAGCTAGAAATAGCAAGTTAA	To generate the sgRNA region of pXY550
50	TCGTATAATGTGCACGCAATTGTCGCCAGAATCTTGTTTTAGAGCTAGAAATAGCAAGTTAA	To generate the sgRNA region of pXY588
51	TGCTGTTGCGTATTGATTATGAAACGCGTCTGGAGAAAGCGCAGGCGTTTGTACGAGGTTCACGAGGTGG	Insertion of *tagrfp-t* gene into chromosomal *ftsW locus*
52	CCACCGGTTCCGCCTGCCATCACCATTAATCGCTTTCCTTGACCACTCATTTACTTGTACAGCTCGTCCATGC	
53	CCGGAAGCGCACACTGACTTTATTTTCGCCTGCATCGGCGAGGAGCTGGGTTATGTCGGTGTGGTGCTGGCACTTTTAATG	Mutagenesis of chromosomal *ftsW* gene to *ftsW*^{I302C}

54	CGCGTGTGCTTGGCTTCGCACGAGACGCAATTGTCTGCCGTATTTTTGGCGCA GGGATGGCAACCGACGCCTTTTTCGTCG	Mutagenesis of chromosomal *murJ* gene to *murJ*^{A29C}
55	TTTCGCCGCTGCTTTCTTGTACAGCTCGTCCATGCC	To generate *tagrfp-t-fts*I without linker and first methionine
56	AAAGCAGCGGCGAAAA	
57	GAGGAGAAATTAACTATGGTGAGCAAAGGCGAAGAAG	Amplification of the *mneongreen* gene
58	GGAGCCAGCGGATCCTTTATACAGTTCATCCATGCCCATC	
59	AGTTAATTTCTCCTCTTTAATGAATTCTG	Amplification of the vector with *zapA* gene for pXY677
60	GGATCCGCTGGCTCCGCTG	

Supplementary Table 3: Quantification of septal NAM labeling.

Percentage of cells with labeled septa	**WT (N)**	***ftsW*^{I302C}**	***Δ3, ponB*^{S247C}**	***Δ3, ponB*^{S247C}, *ftsW*^{I302C}**	***murJ*^{A29C}**
- MTSES	38 ± 4% (1163)	34 ± 4% (970)	32 ± 1% (1128)	29 ± 5% (1200)	32 ± 3% (836)
+ MTSES	32 ± 5% (1113)	22 ± 4% (723)	14 ± 3% (1085)	4 ± 1% (1346)	2.6 ± 0.1% (1031)
R_A (+MTSES/-MTSES)	85 ± 6%	64 ± 5%	42 ± %	13 ± %	9 ± 2%
Integrated Intensity of labeled septa					
- MTSES [a] (a.u)	1.6 ± 0.1×10^6 (442)	1.1 ± 0.1×10^6 (330)	0.6 ± 0.1×10^6 (361)	0.5 ± 0. ×10^6 (348)	0.69 ± 0.03×10^6 (268)
+ MTSES[a] (a.u)	1.5 ± 0.1×10^6 (356)	0.8 ± 0.1×10^6 (160)	0.37 ± 0.07×10^6 (152)	0.18 ± 0.05×10^6 (53)	0.37 ± 0.02×10^6 (27)
R_B (+MTSES/-MTSES)	98± 13%	70 ± 4%	65 ± 12%	41 ± 12%	54 ± 4%
Loss of total labeling [b]	16 ± 15%	56 ± 5%	72 ± 6%	96 ± 2%	95.5 ± 0.5%

Errors are the mean of standard error of three experimental repeats

Cells were grown in M9-glucose at 25^{o}C

N is the number of cells analyzed

[a] Average cell body intensity was subtracted from the integrated intensity of the septal area. Note the median instead of mean integrated intensity was listed in the table and used for calculations due to the skewed distribution toward high intensity values in a small population of cells. See Methods and Extended Data Fig. 3.

[b] Calculated using $(1 - R_A \cdot R_B)$.

Supplementary Table 4: FtsW dynamics in cells with different FtsZ treadmilling speeds

FtsZ mutation	FtsZ speed[a] (nm/s), (N_Z)	*P_moving*[b] (%), (N_{all})[e]	T_s(s)[c] (N_S)[e]	V_1[d] (nm/s), (N)[e]	P_1_V_1[d] (%)	V_2[d] (nm/s)	*FtsW speed*[b] (nm/s)
wt	28.0±1.2 (182)	61.5±1.8 (519)	19.2±1.1 (204)	8.0±0.3 (315)	37.4±11.2	31.9±4.4	22.5±1.6
E238A	23.8±2.9 (37)	61.1±2.7 (155)	22.3±1.7 (65)	7.9±0.4 (90)	43.1±14.5	28.2±9.5	18.8±9.4
E250A	17.4±1.6 (41)	61.4±2.0 (233)	24.7±1.5 (96)	8.4±0.3 (137)	71.2±14.8	27.7±6.8	12.4±8.3
D269A	14.3±1.3 (32)	50.1±2.3 (158)	23.8±1.7 (84)	7.8±0.4 (74)	46.7±22.6	15.7±5.5	11.0±7.1
G105S	9.7±1.0 (35)	47.9±2.1 (219)	26.3±1.5 (112)	7.6±0.5 (102)	34.5±12.7	11.0±1.8	10.3±7.6
D158A	7.4±0.7 (36)	39.2±2.7 (144)	30.6±2.4 (85)	9.0±2.9 (59)	44.9±22.5	12.8±3.7	11.3±9.1

All the experiments were performed with cells growing on M9-glucose medium

[a]FtsZ treadmilling speeds are from[7]. mean ± S.E.M, where S.E.M is the standard error of mean speed. N_z is the number of FtsZ kymograph segments.

[b]Percentage of time (*P_moving*) and average speed of FtsW-RFP molecules spent in directional moving state. Data expressed as mean ± error, where the error is the standard deviation from 1000 bootstrap samples pooled from three independent experiments.

[c]Average dwell time of stationary FtsW-RFP molecules. Data expressed as mean ± S.E.M.

[d]Speed (V_1), percentage (P_1_V_1) of the slow-moving population and speed (V_2) of the fast-moving population of FtsW-RFP obtained from two-population free-float fitting of CDF curves bootstrapped 1000 times from three independent experiments. Errors are the standard deviations of the fitted parameters.

[e]N_{all} is the number of total track segments while N is the number of segments corresponding to a directionally moving molecule and N_s is the number of segments corresponding to a stationary molecule.

Supplementary Table 5: FtsI dynamics in different strains

genotype	medium	*P_moving*[a] (%), (N_{all})[c]	V_1[b] (nm/s), (N)[c]	P_1_V_1[b] (%)	V_2[b] (nm/s)	*FtsI average speed*(nm/s)
BW25113	M9-glucose	54.2±3.7 (92)	9.8±1.1 (52)	53.9±19.9	31.2±5.6	20.2±2.0
BW25113, *ftsZ*^{E250A}	M9-glucose	58.0±4.7 (84)	9.1±1.8 (45)	21.9±22.6	19.2±3.4	16.5±1.7
TB28, *ftsB*^{E56A}	M9-glucose	52.2±3.4 (146)	9.2±0.7 (76)	89.8±4.4	37.3±3.8	12.4±1.4

[a] Percentage of time (*P_moving*) and average speed of RFP-FtsI molecules spent in directional moving state. Data expressed as mean ± error, where the error is the standard deviation of 1000 bootstrap samples from three experiments.

[b] Speed (V_1), percentage (P_1_V_1) of the slow-moving population and speed (V_2) of the fast-moving population of RFP-FtsI obtained from two-population free-float fitting of 1000 CDF curves bootstrapped from three experiments. Errors are the standard deviations of the fitted parameters.

[c] N_{all} is the number of total track segments while N is the number of segments corresponding to a directionally moving molecule.

Supplementary Table 6: FtsW dynamics under different sPG synthesis conditions

genotype	Drug or medium	*P_moving*[b] (%), (N_{all})[f]	T_s[c](s), (N_s)[f]	V_1[c] (nm/s), (N)[f]	$P_1\_V_1$[c] (%)	V_2[c] (nm/s)	*FtsZ speed*[e] (nm/s), (N_z)	*FtsW average speed*(nm/s)
BW25113	EZRDM	63.6±0.8 (1445)	13.6±0.5 (535)	11.1±0.24 (910)	80.7±1.8	51.9±2.3	49.8±2.9 (182)	18.6±0.8
BW25113	M9-glucose	61.5±1.8 (519)	19.2±1.1(204)	8.0±0.3 (315)	37.4±11.2	31.9±4.4	28.0±1.2 (182)	22.5±1.6
BW25113	Fosfomycin, M9-glucose	20.5±1.3 (643)	15.2±0.8(404)	9.6±0.1 (239)	7.9±9.3	34.9±2.9	39.7±1.9 (192)	31.4±1.6
BW25113	Aztreonam, M9-glucose	11.1±3.4 (347)	24.6±1.4(245)	9.2±0.1 (102)	19.8±7.7	34.6±2.0	39.2±2.1 (197)	29.9±2.0
BW25113, *ftsW*^{I302C}	M9-glucose	52.4±1.8 (361)	18.2±1.0 (169)	10.7±0.9 (192)	55.4±7.5	33.8±2.7	38.6±3.2 (85)	20.7±1.8
BW25113, *ftsW*^{I302C}	MTSES, M9-glucose	38.0±1.2 (757)	20.1±0.7 (418)	10.4±2.5 (339)	43.4±9.1	30.0±2.4	35.1±2.0 (85)	22.5±1.3
MG1655,Δ3 ponB^{S247C} *ftsW*^{I302C}	M9-glucose	46.7±2.1 (499)	11.9±0.9(223)	9.2±0.1 (276)	16.5±6.2	32.1±1.5	42.3±2.1 (166)	26.5±1.5
MG1655,Δ3 ponB^{S247C} *ftsW*^{I302C}	MTSES, M9-glucose	19.6±1.8 (363)	18.9±1.9(206)	9.1±0.2 (157)	1.2±2.7	32.1±1.5	38.1±2.8 (98)	33.9±2.3
TB28	M9-glucose	44.8±1.7 (477)	18.2±0.8(258)	9.4±0.3 (219)	63.6±7.6	37.8±6.1	ND[a]	18.8±1.6
MG1655, P_{BAD}::*ftsN*	M9-glucose[d]	31.4±1.0 (1094)	16.3±0.6(696)	10.5±0.8 (398)	41.7±14.7	30.1±3.9	ND[a]	22.1±1.3
TB28, *ftsB*^{E56A}	M9-glucose	36.3±1.6 (499)	20.3±0.8(323)	9.3±0.8 (176)	93.3±3.7	46.9±8.4	50.2±2.4 (180)	11.7±1.1
TB28, *ΔftsN*, *ftsB*^{E56A}	M9-glucose	36.0±1.7 (339)	23.4±1.3 (195)	7.9±0.6 (144)	76.2±4.4	56.2±2.7	ND[a]	18.2±2.3
TB28, *ftsW*^{E289G}	M9-glucose	49.8±1.7 (383)	18.2±1.0 (107)	8.9±0.9 (176)	79.1±5.6	35.4±3.7	ND[a]	13.9±1.1

TB28, *ftsI*^{R167S}	M9-acetate	35.6±1.3 (756)	19.4±0.6(496)	6.2±0.5 (260)	55.6±4.8	28.7±2.7	31.6±2.0 (84)	16.8±1.5
TB28, *ftsI*^{R167S}	M9-glucose	60.6±1.3 (491)	17.6±0.7(236)	6.4±0.2 (255)	90.7±2.1	37.2±1.0	36.8±2.3 (92)	8.8±0.6
TB28, *ftsI*^{R167S}	EZRDM	60.1±2.2 (173)	12.0±0.9(81)	11.3±0.7 (92)	87.5±5.5	40.0±1.5	37.2±2.8 (83)	14.5±1.4
TB28, *ftsI*^{R167S}	EZRDM+UppS	55.7±1.1 (954)	11.1±0.4(441)	13.2±0.3 (513)	93.9±2.2	40.0±1.4	ND[a]	14.5±0.4
TB28, *ftsI*^{R167S}	1XPBS (4% PFA fixed)	2.3±0.4 (182)	NA[a]	NA[a]	NA[a]	NA[a]	NA[a]	33.6±3.3

[a] N.A. not applicable. N.D. not measured

[b] Percentage of time (*P_moving*) and average speed of FtsW-RFP molecules spent in directional moving state. Data expressed as mean ± error, where the error is the standard deviation of 1000 bootstrap samples from three experiments.

[c] Speed (V_1), percentage (P_1_V_1) of the slow-moving population and speed (V_2) of the fast-moving population of FtsW-RFP obtained from two-population free-float fitting of 1000 CDF curves bootstrapped from three experiments. Errors are the standard deviations of the fitted parameters.

[d] Medium without arabinose (FtsN-depleted).

[e] FtsZ's treadmilling speed, mean ± S.E.M, where S.E.M is the standard error of mean speed. N_z is the number of FtsZ kymograph segments.

[f] N_{all} is the number of total track segments while N is the number of segments corresponding to a directionally moving molecule and N_s is the number of segments corresponding to a stationary molecule.

Supplementary Table 7. Superfission variants of FtsB, FtsI or FtsW cause a short-cell phenotype, and can rescue Δ*ftsN* cells.

Row[a]	Strain	Genotype	*Td*[b]	*N*[c]	Average length		Average width		Average volume	
					µm (SD)	%WT	µm (SD)	%WT	µm (SD)	% WT
LB										
1	TB28	wt	41	303	4.42 (1.07)	100	0.95 (0.06)	100	2.91 (0.76)	100
2	BL167	*ftsB*^{E56A}	45	324	3.42 (0.82)	77	1.05 (0.07)	110	2.65 (0.71)	91
3	BL173	*ftsB*^{E56A} Δ*ftsN*	45	235	9.87 (4.56)	235	0.92 (0.05)	97	6.38 (3.19)	219
4	PM17	*ftsW*^{E289G}	43	331	3.40 (0.74)	81	1.00 (0.07)	105	2.40 (0.65)	82
5	PM18	*ftsW*^{E289G} Δ*ftsN*	43	343	6.28 (1.79)	142	0.96 (0.05)	101	4.27 (1.32)	147
6	PM6	*ftsI*^{R167S}	43	283	3.53 (0.80)	80	0.98 (0.07)	103	2.40 (0.63)	82
7	PM8	*ftsI*^{R167S} Δ*ftsN*	N.A[d]. Cells not viable							
M9-glucose										
8	TB28	wt	99	333	2.62 (0.57)	100	1.01 (0.08)	100	1.82 (0.46)	100
9	BL167	*ftsB*^{E56A}	101	363	2.10 (0.44)	80	1.08 (0.08)	107	1.60 (0.39)	88
10	BL173	*ftsB*^{E56A} Δ*ftsN*	101	288	5.45 (2.24)	208	0.94 (0.06)	93	3.56 (1.46)	196
11	PM17	*ftsW*^{E289G}	98	307	2.41 (0.58)	92	1.06 (0.07)	105	1.80 (0.47)	99
12	PM18	*ftsW*^{E289G} Δ*ftsN*	93	349	4.56 (1.06)	174	0.97 (0.08)	96	3.15 (0.88)	173
13	PM6	*ftsI*^{R167S}	100	336	2.20 (0.44)	84	1.06 (0.09)	105	1.60 (0.39)	88
14	PM8	*ftsI*^{R167S} Δ*ftsN*	N.A[d], cells are viable but grow poorly and are very filamentous							

[a] Cells were grown at 30°C. Overnight cultures were diluted to OD_{600} = 0.02 in LB and grown to OD_{600} = 0.6-0.7 (rows 1-6), or to OD_{600} = 0.05 in M9-glucose and grown to OD_{600} = 0.5-0.6 (rows 8-13). Cells were then chemically fixed, imaged with phase-contrast optics, and measured using MicrobeJ software[16].

[b] Mass doubling time in minutes.

[c] Number of cells measured.

[d] N.A. not available

Supplementary Table 8. Growth and constriction rates of TB28, *ftsI*^{R167S} cells.

medium	*Doubling Time*[a] (min)	*Constriction rate* [c] (nm/min), (*N*)[d]
M9-acetate	806±20[b]	5.6±0.8[e] (13)
M9-glucose	202±9	17.2±1.9 (15)
M9-EZRDM	57.2±3.8	37.9±2.0 (16)
M9-EZRDM+UppS	NA	39.7±2.3 (20)

[a] Mass doubling time in minutes at 25ºC in liquid culture.

[b] mean ± s.d. of 2 independent experiments.

[c] Constriction rates on gel-pad at ~ 25ºC

[d] Number of cells measured.

[e] mean ± S.E.M. of all cells from 2-3 independent experiments.

Supplementary Table 9. Mean Error of single- and double-population fitting of CDF curves.

genotype	Drug or medium	*Error_1*[a]	*Error_2*[b]	genotype	Drug or medium	*Error_1*[a]	*Error_2*[b]
FtsW-RFP							
BW25113	EZRDM	0.012	0.0031	BW25113, ftsZE238A	M9-glucose	0.015	0.0089
BW25113	M9-glucose	0.014	0.0037	BW25113, ftsZE250A	M9-glucose	0.010	0.0052
BW25113	Fosfomycin, M9-glucose	0.0060	0.0051	BW25113, ftsZD269A	M9-glucose	0.013	0.0088
BW25113	Aztreonam, M9-glucose	0.0081	0.0049	BW25113, ftsZG105S	M9-glucose	0.010	0.0066
BW25113, *ftsW*^{I302C}	M9-glucose	0.0122	0.0040	BW25113, ftsZD158A	M9-glucose	0.011	0.0075
BW25113, *ftsW*^{I302C}	MTSES, M9-glucose	0.0060	0.0033	MG1655, PBAD::ftsN	M9-glucose	0.0046	0.0039
MG1655,Δ3 ponB^{S247C} *ftsW*^{I302C}	M9-glucose	0.0070	0.0037	TB28, ftsBE56A	M9-glucose	0.0079	0.0048
MG1655,Δ3 ponB^{S247C} *ftsW*^{I302C}	MTSES, M9-glucose	0.0062	0.0046	TB28, ΔftsN, ftsBE56A	M9-glucose	0.0160	0.0061
TB28	M9-glucose	0.0125	0.0047	TB28, *ftsW*^{E289G}	M9-glucose	0.0098	0.0048
TB28, *ftsI*^{R167S}	M9-glucose	0.0105	0.0032	TB28, *ftsI*^{R167S}	EZRDM	0.0103	0.0051
TB28, *ftsI*^{R167S}	M9-acetate	0.0130	0.0048	TB28, *ftsI*^{R167S}	EZRDM +UppS	0.0063	0.0051
RFP-FtsI							
BW25113	M9-glucose	0.013	0.0060	BW25113, ftsZE250A	M9-glucose	0.010	0.0058
TB28, ftsBE56A	M9-glucose	0.011	0.0057				

[a] mean CDF fitting error of single population log-normal distribution. The mean error is calculated as:

$$\langle Error \rangle = < \frac{1}{N} \sum_{i=1}^{N} \sqrt{R_i^2} >$$

Where R_i is the residual of data point i of the CDF curve.

[b] mean CDF fitting error of double-population log-normal distribution. The mean error is calculated as in[a].

Discussion:

Functionality of FtsW-TagRFP-t construct

We verified that the chromosomal replacement of *ftsW* with the *ftsW-rfp* allele (strain JXY422) still supports cell growth similar to BW25113 in both LB and M9-glucose media (Supplementary Fig. 1a-b). FtsW-RFP is also expressed without observable degradation (Supplementary Fig. 1g) and localizes correctly to midcell where sPG synthesis taking place (Supplementary Figure 1f).

The processive motion and confined diffusion of FtsW-RFP are not imaging artifacts

To rule out the possibility that the movement we observed arises from some imaging artifacts such as mechanical drift of the sample, we imaged fixed cells under our typical condition. In those cells, only 2.3 ± 0.4% of the molecules exhibited directional movement using the same data processing pipeline. This is 4~5-fold lower than under the Aztreonam treated condition that has the least directional moving trajectories, indicating that any imaging artifact is negligible (Supplementary Table 6). As expected, the MSD curve of the trajectories in fixed sample also showed a much tighter confinement than that of stationary FtsW-RFP in WT cells but similar to that of the Aztreonam treated cells, suggesting two types of stationary populations (Extended Data Fig. 3c).

Classification of single molecule segments

As shown in Extended Data Fig. 5e, we can linearly fit a single molecule trajectory (segment) with T frames to estimate the speed V and calculate the standard deviation of fitting residuals S, while the ground truth of the speed is $\hat{V}$. The confidence of calling one segment as in directional motion depends on the related level of S, which is a function of the localization error, diffusion coefficient and confinement size. We further defined a dimensionless metric R that is S normalized by the total displacement of the segment $L =$

$T \cdot V$. Thus, the classification problem can be described as estimating the probability of the segment to be 'stationary' given T and R:

$$P_s = P(Stationary|T,R) \approx P\left(\hat{V} = 0 \middle| T,R\right) \quad (1)$$

And the probability of directional movement is

$$P_m = P(processive|T,R) \approx P\left(\hat{V} = V \middle| T,R\right) \quad (2)$$

Here, we simplified the problem to a binary classification with two most likely speeds, 0 or V. We developed the following algorithm to calculate the probabilities in (1) and (2) and to classify a certain segment as stationary or directional moving.

Step 1: build the probability density function (PDF) of R from simulation

Since R is defined as $\frac{S}{T \cdot V}$, where S depends on the localization error (δ), diffusion coefficient (D) and confinement size (B), we first determined $\delta_0 = 37nm, D_0 = 0.0007$ μm^2/s, $B_0 = 95\ nm$ of FtsW-RFP under our experimental condition from the MSD fitting results shown in Extended Data Fig. 7c. Note that we simulated stationary RFP-FtsI molecules' PDF using the same parameter set since FtsI is expected to be in the same complex and displays similar motion as FtsW-RFP. For an experimental segment with length T_{exp} and fit speed V_{fit}, we carried out two sets of random simulations to generate 1000 segments based on fixed $\delta_0, D_0,\ B_0,\ T_{exp}$, and $V = 0\ or\ V_{fit}$. All the simulated segments were then fit linearly to calculate their R values. The distribution was used to construct the PDF of R given a stationary or directional movement state:

$$PDF_s(R) = PDF\left(R \middle| \delta_0, D_0, B_0, T_{exp}, V = 0\right) \quad (3)$$

$$PDF_m(R) = PDF\left(R \middle| \delta_0, D_0, B_0, T_{exp}, V = V_{fit}\right) \quad (4)$$

Step 2: Estimate the experimental distribution of R_{exp}:

We determined the distribution of R_{exp} using a bootstrapping-like procedure. We first randomly deleted 10% of the datapoints from the segment for 100 times. We then fit all the re-sampled segments by line and calculated the corresponding standard error (σ) of R_{exp}. Next, we integrated $\langle R_{exp}\rangle \pm \sigma$ in (3) and (4) to obtain the probability of R_{exp} given the conditions described above and the speed.

$$P\left(R_{exp}\middle|stationary\right) = \int_{\langle R_{exp}\rangle-\sigma}^{\langle R_{exp}\rangle+\sigma} P\left(R\middle|\delta_0, D_0, B_0, T_{exp}, V=0\right)dR \quad (5)$$

$$P\left(R_{exp}\middle|processive\right) = \int_{\langle R_{exp}\rangle-\sigma}^{\langle R_{exp}\rangle+\sigma} P\left(R\middle|\delta_0, D_0, B_0, T_{exp}, V=V_{fit}\right)dR \quad (6)$$

Step 3: Bayesian inference:

For every segment, we calculated its P_m using Bayes' theorem:

$$P_m = \frac{P\left(R_{exp}\middle|processive\right)P(processive)}{P\left(R_{exp}\middle|stationary\right)P(Stationary) + P\left(R_{exp}\middle|processive\right)P(processive)}$$

$$= \frac{P\left(R_{exp}\middle|processive\right)}{P\left(R_{exp}\middle|stationary\right) + P\left(R_{exp}\middle|processive\right)}$$

Here we assume no prior knowledge on the type of motion, thus $P(stationary) = P(processive)$.

Step 4: Classification:

We used a set of thresholds: $P_m > 0.75$ and $R_{exp} < 0.4$ to identify directional or processive moving molecules, which is comparable with a manual classification but largely reduced the potential systematic bias.

Estimation of PG synthesis rate in E. coli

Burman et al.[17] estimated that *E. coli* cells growing with a doubling time of 48 min, insert about 450,000 new muropeptides in the peptidoglycan sacculus during an 8-min labeling period with radioactive cell wall precursors. This is equivalent to 150 PG loops

around the cell circumference (each loop corresponds to ~ 3000 muropeptides or 3000 nm). If one assumes that there are ~150 PG synthase complexes[18] that simultaneously synthesize the PG in a processive fashion, the polymerization rate for each loop would be 3000 nm / 480 s = 6 nm/s. Note that this number is lower than the directional moving speed of the RodA/PBP2 system for cell wall elongation[6] , and that this simplified estimation does not take into account the number of enzyme molecules presented on each loop's synthesis, the contribution of other PGTases, the growth condition (our growth condition is at RT and in minimal media), and the simultaneous PG turnover process. Nevertheless, the speed estimated from these labeling experiments and the speed of the RodA system agree with our SMT measurements in the same order of magnitude.

Captions for Movies

MovieS1:

Phase contrast time-lapse movie of JXY559 (BW25113 *ftsW*^{I302C}) cells growing on 3% agarose gel-pad with M9-glucose minimum medium in the absence of MTSES at room temperature. The movie was recorded every ~3.5 minutes Scale bar: 5 μm.

MovieS2:

Phase contrast time-lapse movie of JXY559 (BW25113 *ftsW*^{I302C}) cells growing on 3% agarose gel-pad with M9-glucose minimum medium at room temperature. The gel-pad was supplemented with 0.1mM MTSES. The movie was recorded every ~3.5 minutes Scale bar: 5 μm.

MovieS3-9:

Epi-fluorescence time-lapse imaging of single FtsW-RFP molecules in M9-glucose, corresponding to Extended Data Fig. 3a, Fig. 2a, b, and Extended Data Fig. 2a-d. Frame rate = 2 frames/second; camera pixel size = 81.25 nm. Scale bar: 0.5 μm.

Reference:

1.Buss, J. *et al.* A multi-layered protein network stabilizes the Escherichia coli FtsZ-ring and modulates constriction dynamics. *PLoS Genet* **11,** e1005128 (2015).

2.Tarry, M. *et al.* The Escherichia coli cell division protein and model Tat substrate SufI (FtsP) localizes to the septal ring and has a multicopper oxidase-like structure. *J Mol Biol* **386,** 504–519 (2008).

3.Datsenko, K. A. & Wanner, B. L. One-step inactivation of chromosomal genes in Escherichia coli K-12 using PCR products. *Proc Natl Acad Sci USA* **97,** 6640–6645 (2000).

4.Liu, B., Persons, L., Lee, L. & de Boer, P. A. J. Roles for both FtsA and the FtsBLQ subcomplex in FtsN-stimulated cell constriction in Escherichia coli. *Mol Microbiol* **95,** 945–970 (2015).

5.Gerding, M. A. *et al.* Self-enhanced accumulation of FtsN at Division Sites and Roles for Other Proteins with a SPOR domain (DamX, DedD, and RlpA) in Escherichia coli cell constriction. *J Bacteriol* **191,** 7383–7401 (2009).

6.Cho, H. *et al.* Bacterial cell wall biogenesis is mediated by SEDS and PBP polymerase families functioning semi-autonomously. *Nat Microbiol* **1,** 16172 (2016).

7.Yang, X. *et al.* GTPase activity-coupled treadmilling of the bacterial tubulin FtsZ organizes septal cell wall synthesis. *Science* **355,** 744–747 (2017).

8.Guyer, M. S., Reed, R. R., Steitz, J. A. & Low, K. B. Identification of a sex-factor-affinity site in E. coli as gamma delta. *Cold Spring Harb Symp Quant Biol* **45 Pt 1,** 135–140 (1981).

9.Bernhardt, T. G. & de Boer, P. A. J. The Escherichia coli amidase AmiC is a periplasmic septal ring component exported via the twin-arginine transport pathway. *Mol Microbiol* **48,** 1171–1182 (2003).

10.Guzman, L. M., Belin, D., Carson, M. J. & Beckwith, J. Tight regulation, modulation, and high-level expression by vectors containing the arabinose PBAD promoter. *J Bacteriol* **177,** 4121–4130 (1995).

11.Liang, H. *et al.* Metabolic labelling of the carbohydrate core in bacterial peptidoglycan and its applications. *Nat Commun* **8,** 15015 (2017).

12.Hale, C. A. & de Boer, P. A. J. ZipA is required for recruitment of FtsK, FtsQ, FtsL, and FtsN to the septal ring in Escherichia coli. *J Bacteriol* **184,** 2552–2556 (2002).

13.Mercer, K. L. N. & Weiss, D. S. The Escherichia coli cell division protein FtsW is required to recruit its cognate transpeptidase, FtsI (PBP3), to the division site. *J Bacteriol* **184,** 904–912 (2002).

14.Cho, H., Uehara, T. & Bernhardt, T. G. Beta-lactam antibiotics induce a lethal malfunctioning of the bacterial cell wall synthesis machinery. *Cell* **159,** 1300–1311 (2014).

15.Lyu, Z., Coltharp, C., Yang, X. & Xiao, J. Influence of FtsZ GTPase activity and concentration on nanoscale Z-ring structure in vivo revealed by three-dimensional Superresolution imaging. *Biopolymers* **105,** 725–734 (2016).

16.Ducret, A., Quardokus, E. M. & Brun, Y. V. MicrobeJ, a tool for high throughput bacterial cell detection and quantitative analysis. *Nat Microbiol* **1,** 16077 (2016).

17.Burman, L. G. & Park, J. T. Molecular model for elongation of the murein sacculus of Escherichia coli. *Proc Natl Acad Sci USA* **81,** 1844–1848 (1984).

18.Egan, A. J. F. & Vollmer, W. The stoichiometric divisome: a hypothesis. *Front Microbiol* **6,** 455 (2015).